Human Molecular Genetics, 2020, Vol. 29, No. 19 3285–3295

doi: 10.1093/hmg/ddaa210
Advance Access Publication Date: 25 September 2020
General Article

GENERAL ARTICLE

Specific ZNF274 binding interference at *SNORD116* activates the maternal transcripts in Prader-Willi syndrome neurons

Maéva Langouët[1,†], Dea Gorka[1], Clarisse Orniacki[1], Clémence M. Dupont-Thibert[1], Michael S. Chung[1], Heather R. Glatt-Deeley[1], Noelle Germain[1], Leann J. Crandall[1], Justin L. Cotney[1,2], Christopher E. Stoddard[1], Marc Lalande[1,2] and Stormy J. Chamberlain[1,2,*]

[1]Department of Genetics and Genome Sciences, University of Connecticut School of Medicine, Farmington, CT 06030, USA and [2]Institute for Systems Genomics, University of Connecticut, Farmington, CT 06030, USA

*To whom correspondence should be addressed at: Department of Genetics and Genome Sciences, UCONN Health, Farmington, CT 06030, USA. Tel: +1 860 679 4433; Fax: +1 860 679 8345; Email: chamberlain@uchc.edu

Abstract

Prader-Willi syndrome (PWS) is characterized by neonatal hypotonia, developmental delay and hyperphagia/obesity. This disorder is caused by the absence of paternally expressed gene products from chromosome 15q11–q13. We previously demonstrated that knocking out ZNF274, a Kruppel-associated box-A-domain zinc finger protein capable of recruiting epigenetic machinery to deposit the H3K9me3 repressive histone modification, can activate expression from the normally silent maternal allele of *SNORD116* in neurons derived from PWS induced pluripotent stem cells (iPSCs). However, ZNF274 has many other targets in the genome in addition to *SNORD116*. Depleting ZNF274 will surely affect the expression of other important genes and disrupt other pathways. Here, we used CRISPR/Cas9 to delete ZNF274 binding sites at the *SNORD116* locus to determine whether activation of the maternal copy of *SNORD116* could be achieved without altering ZNF274 protein levels. We obtained similar activation of gene expression from the normally silenced maternal allele in neurons derived from PWS iPSCs, compared with ZNF274 knockout, demonstrating that ZNF274 is directly involved in the repression of *SNORD116*. These results suggest that interfering with ZNF274 binding at the maternal *SNORD116* locus is a potential therapeutic strategy for PWS.

Introduction

Prader-Willi syndrome (PWS; OMIM 176270) is a neurogenetic disorder of genomic imprinting and has an incidence of ∼1/15 000 live births. Children affected with PWS suffer neonatal hypotonia and failure-to-thrive during infancy, followed by hyperphagia/obesity; small stature, hands and feet; mild to moderate cognitive deficit and behavioral problems that are likened to obsessive–compulsive disorder. PWS most commonly results from large deletions mediated by repetitive sequences flanking a ∼5 Mb imprinted region on paternal chromosome 15q11–q13 (1,2). There is no cure for PWS. Current treatments focus on alleviation of individual symptoms (3–8).

[†]Maéva Langouët, http://orcid.org/0000-0001-7176-0427
Received: May 21, 2020. **Revised:** July 15, 2020. **Accepted:** August 26, 2020

Many genes in the chromosome 15q11–q13 region are regulated by genomic imprinting. Most genes, including *SNRPN* (a bicistronic transcript that also encodes *SNURF*, referred to henceforth as *SNRPN* only), *SNHG14*, *MKRN3*, *MAGEL2* and *NDN* are exclusively expressed from the paternally inherited allele. *UBE3A* is biallelic in most tissues, but in neurons, this gene is expressed from the maternally inherited allele only. *SNHG14*, a transcriptional unit comprised of several long and short non-coding ncRNAs initiates at the canonical and upstream promoters of *SNRPN* on the paternal allele (Fig. 1). Alternative polyadenylation of *SNHG14* contributes to the neuron-specific expression of *UBE3A-ATS*, a transcript which extends distally and overlaps *UBE3A* in an antisense fashion; therefore, silencing the paternal *UBE3A* allele (9–17). *SNHG14* also serves as the host gene (HG) to several box C/D class small nucleolar RNAs, organized in large, tandemly repeated clusters, known as the *SNORD116* and *SNORD115* clusters (9,17). The 30 copies of the *SNORD116* cluster have been subdivided into three groups based on DNA sequence similarity (18); Group 1 (*SNOG1*, *SNORD116* 1–9), Group 2, (*SNOG2*, *SNORD116* 10–24) and Group 3 (*SNOG3*, *SNORD116* 25–30). The PWS-Imprinting Center (PWS-IC), a region of differential CpG methylation, located in the promoter and first exon of *SNRPN*, is known to control imprinting at this region (19).

Although the genes involved in PWS have been known for many years, the exact contribution of each gene to the symptoms of PWS remains unclear. Efforts have been made to elucidate the targets of PWS snoRNAs: *SNORD115* is thought to regulate splicing (20–22) and A-to-I RNA editing (23–25) of the serotonin HTR2C receptor and *SNORD116* has been computationally predicted to interact with *ANKRD11* mRNA, and perhaps other transcripts (20). Additionally, Keshavarz *et al*. demonstrated a correlation between copy number variation of *SNORD115* and *SNORD116* and behavioral traits, by assessing anxiety both in rodents and humans (26).

In the past decade, focus has shifted to *SNORD116* because recently identified patients with atypical, shorter deletions suggest that most features of PWS could result from the loss of the *SNORD116* snoRNA cluster (27–30). Additionally, mouse models produced by deletion of the *Snord116* cluster show several features of PWS including postnatal growth retardation, increased body weight gain and hyperphagia (31–33). Although the food intake phenotype was recently questioned in a *Snord116* KO mouse model (34), altogether those studies further support the association between *Snord116* and PWS. Moreover, recent work also demonstrated that loss of *SNORD116* in both human induced pluripotent stem cell (iPSC) and mouse models of PWS can lead to a deficiency of prohormone convertase PC1, an intriguing observation that may link *SNORD116* to the neuroendocrine dysfunction in PWS (35,36). However, whether the absence of *SNORD116* genomic region alone, its host-gene lncRNA transcript, the processed snoRNAs and/or simply the active transcription event itself rather than the genomic region/RNA products is responsible of the disease remains an active debate.

Since every individual with PWS has a functional copy of the genetic region that is epigenetically silenced, activation of these genes offers an attractive therapeutic approach for this disorder.

Using our PWS and Angelman Syndrome (AS) iPSC models, we previously reported that the Kruppel-associated box-A-domain zinc finger protein ZNF274 binds to six sites on the maternal copy of the *SNORD116* cluster where it associated with the histone methyltransferase, SETDB1, and mediates the deposition of the repressive H3K9me3 chromatin mark on the maternal allele (37–39). By knocking out *ZNF274*, we were able to activate the silent maternal allele in PWS iPSC-derived neurons, without affecting DNA methylation at the PWS-IC (40). These results suggested that the ZNF274 complex mediates a separate imprinting mark that represses maternal PWS gene expression in neurons. Genome-wide *ZNF274* depletion, however, does not represent an ideal therapeutic strategy since ZNF274 may have crucial functions outside the PWS locus (41). Here, we deleted and mutated the ZNF274 binding sites (BS) within the *SNORD116* locus in human PWS iPSCs. We found that preventing ZNF274 from binding leads to activation of maternal copies of PWS genes in human PWS iPSC-derived neurons. This demonstrates that *SNORD116* is a direct target of ZNF274-mediated repression. A strategy to inhibit binding of ZNF274 specifically at the maternal *SNORD116* region could potentially restore gene expression from the maternal copies of the PWS genes, while not affecting the other ZNF274-bound loci, providing what may be an optimal therapeutic approach for PWS.

Results

Identification of the *ZNF274* consensus binding motif

In order to design strategies to block ZNF274 binding at *SNORD116*, we developed a computational approach to search for a consensus DNA BS for ZNF274. We analyzed 21 ZNF274 chromatin immunoprecipitation followed by sequencing (ChIP-Seq) datasets from eight different cultured cell lines performed by the ENCODE Consortium and identified 1572 reproducibly bound sites in the human genome. We extracted the sequence of each of these sites from the reference human genome and analyzed this set with the Multiple Em for Motif Elicitation (MEME) suite (42). We were able to identify a single binding motif for ZNF274 (Fig. 2A). Using this consensus binding motif, we then predicted all ZNF274 BSs genome-wide using the Find Individual Motif Occurrences (FIMO) (43) routine from the MEME suite (42). The best match to the consensus ZNF274 motif elicited from ChIP-Seq data (TGAGTGAGAACTCATACC) was identified five times within the *SNORD116* cluster (Fig. 3A). Another group independently identified a putative ZNF274 binding motif. (44) This motif is similar to ours, and is only shifted 2 bp downstream (Fig. 3A). The *SNORD116* cluster is comprised of 30 copies of the snoRNA and can be classified into three groups based on DNA sequence similarity (18). Group 1 consists of *SNORD116*–1 through *SNORD116*-9 (Fig. 1). The exact ZNF274 motif was identified in five of the nine copies of *SNORD116* within this group, *SNORD116*-3, -5, -7, -8 and -9 (Fig. 2B). *SNORD116*-1 contains a single nucleotide change (at position 17) from the ZNF274 consensus binding motif (Fig. 3A). ChIP-Seq data indicate that the binding here is less reproducible, suggesting that this single nucleotide change may reduce ZNF274 binding affinity (Fig. 2B). Nonetheless, in human pluripotent stem cells, ZNF274 binds to all six predicted ZNF274 BSs within *SNORD116*, as determined by ChIP-seq and ChIP-qPCR (37,40), despite the single nucleotide change. *SNORD116*-2, -4 and -6 each display a G-to-A substitution at position 8 in the consensus motif (in magenta, Fig. 3A) and were not identified as being bound by ZNF274 in ChIP-Seq data. The consensus binding motif was also found in all nine Group 1 *SNORD116* copies in the cynomolgus monkey (*Macaca fascicularis*) genome, and all have a G at the position 8 of the motif. We confirmed ZNF274 binding at three *SNORD116* copies in cynomolgus iPSCs by ChIP-qPCR (Fig. 2C). This demonstrates the conservation of the ZNF274 consensus

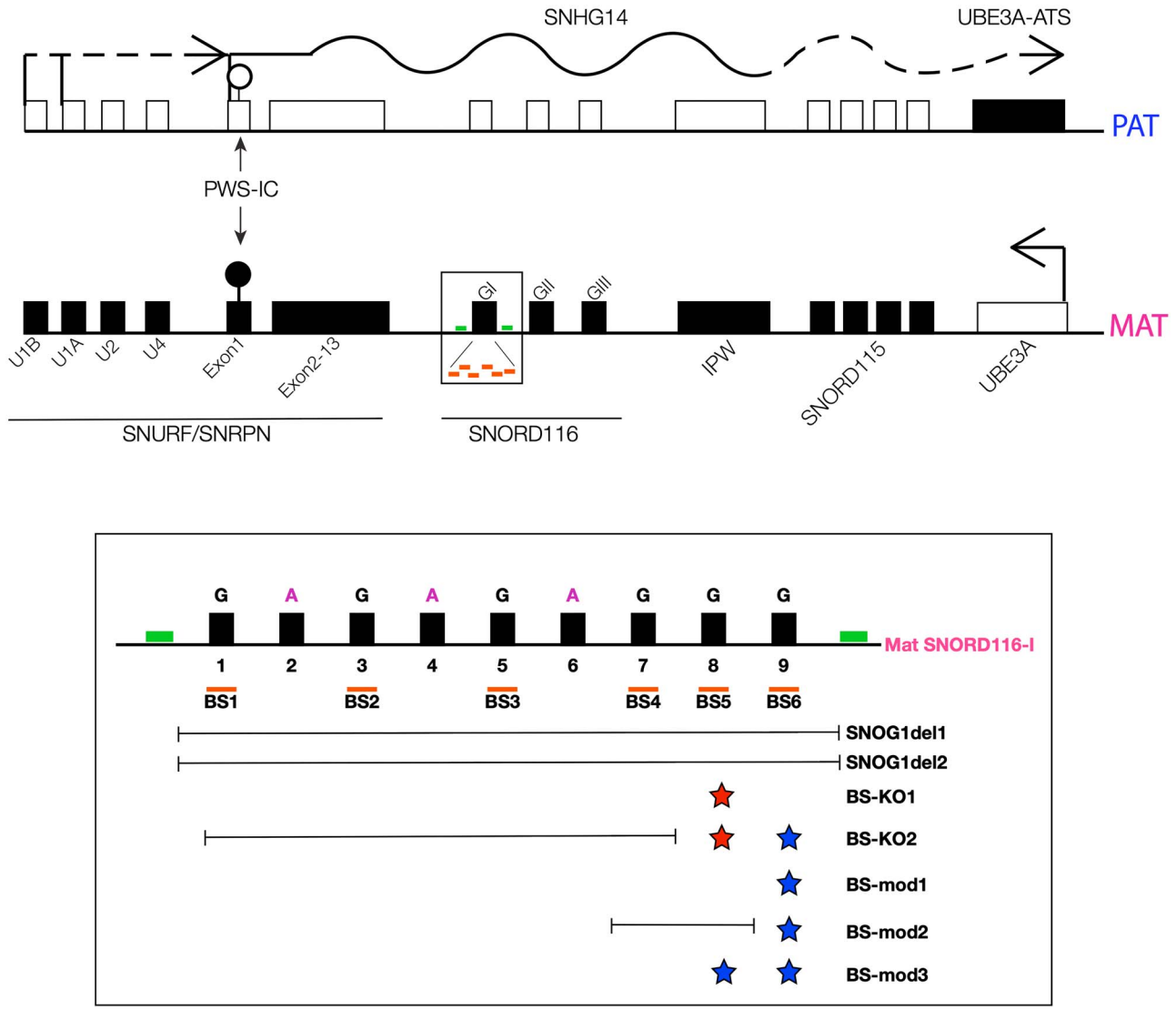

Figure 1. Summary of ZNF274 BS modifications at the *SNORD116* locus. Simplified map of 15q11.2–q13. Active and inactive transcripts are denoted by open and closed boxes, respectively. Arrows indicate the direction of transcription. A solid black line represents paternal *SNHG14* transcript expressed in most cell types, whereas a dashed black line indicates neuron-specific transcripts, including upstream exons of *SNRPN* and *UBE3A-ATS*. The PWS-IC is denoted by the black (methylated)/white (un-methylated) circle. Orange dashes under the *SNORD116* cluster represent the six ZNF274 BSs within the *SNORD116*s classified as Group 1 (*SNOG1-BS1* to *SNOG1-BS6*). Positions of SNOG1del Guide-1 and -2 are indicated with green dashes, surrounding *SNORD116*. In the zoomed area below, positions of large deletions spanning multiple or all the six ZNF274 BSs are indicated, as well as each mutation (red star) or modification (blue star) described in each cell line generated in this paper.

binding motif in primates and further suggests the importance of the G nucleotide at position 8.

Generation of PWS iPSCs cell lines with modified ZNF274 binding sites

To determine whether disruption of the ZNF274 BSs within the *SNORD116* cluster would lead to activation of maternal *SNORD116* in PWS neurons, we used CRISPR/Cas9 to delete or modify one or several BS, starting from our PWS cell line harboring a large deletion of paternal 15q11–q13.

First, we used two guide RNAs (gRNAs; SNOG1del Guide-1 and SNOG1del Guide-2) to delete the entire cluster of six ZNF274 BSs (i.e. SNOG1 region) in PWS iPSCs. We analyzed two independent clones with this deletion, SNOG1-del1 and SNOG1-del2 (Fig. 1 and Supplementary Material, Table S2).

Second, we used the unique sequence flanking the consensus binding motif at each of the six ZNF274 BSs to specifically mutate the sites within the *SNORD116* cluster. We designed two different gRNAs to target Cas9 to these ZNF274 binding motifs. 116-Z-BS Guide 1, which uses the canonical SpCas9 and a NGG protospacer adjacent motif (PAM), is able to target *SNORD116*–2 to 9 (Fig. 3A, blue box and Supplementary Material, Table S1). This was expressed transiently in PWS 1–7 iPSCs. 116-Z-BS Guide 2, which uses the VQR variant of SpCas9 and a modified PAM sequence NGNG/NGAN, was introduced using a lentiviral vector. The PAM sequence for this CRISPR encompassed the crucial G-to-A change in the consensus binding motif, allowing us to target all of the ZNF274 BSs at the locus without affecting the non-ZNF274 binding motifs at *SNORD116*–2, −4 and − 6 (Fig. 3A, red box and Supplementary Material, Table S1).

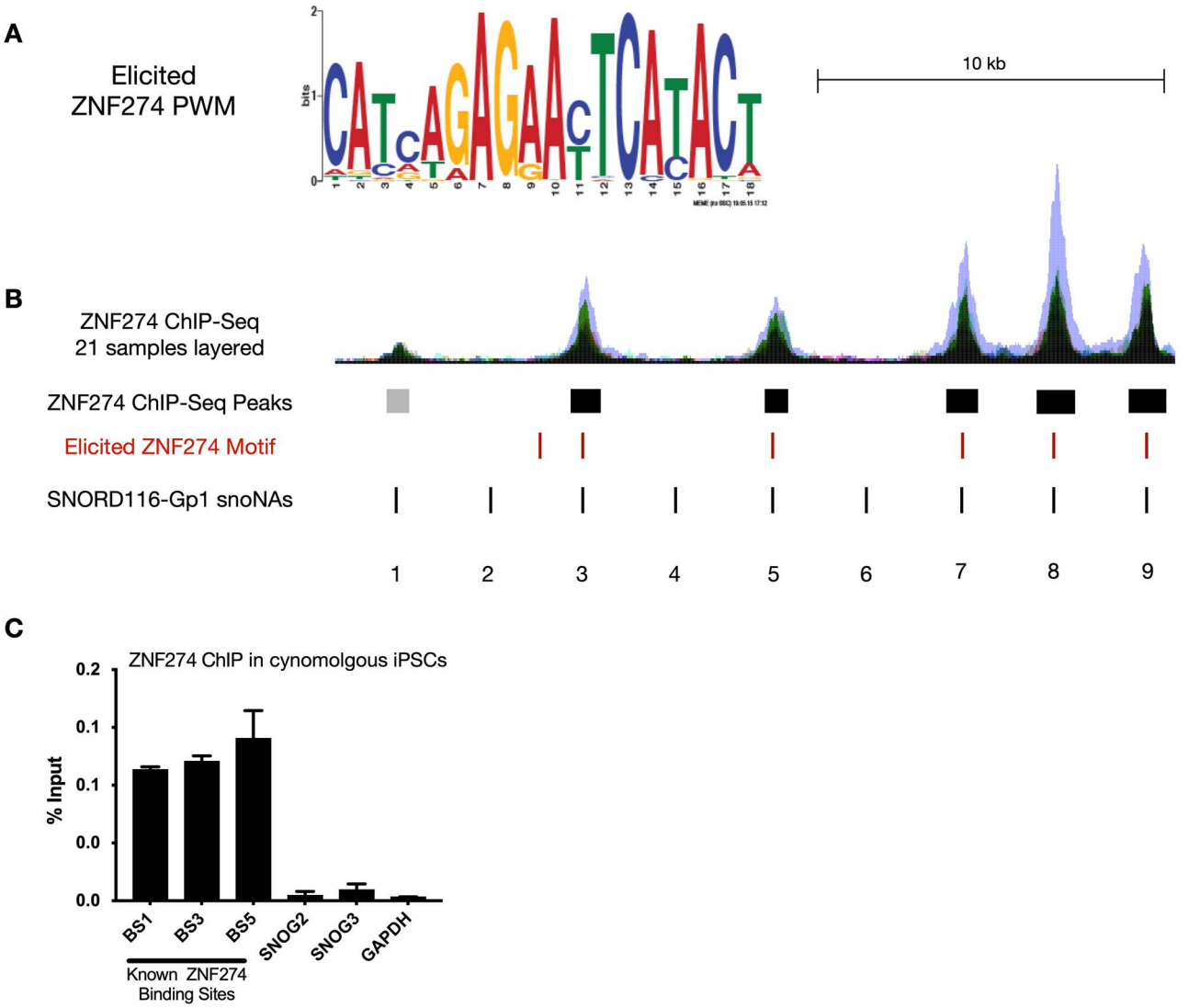

Figure 2. Region of nucleotide homology surrounding the ZNF274 motif at *SNORD116*. (**A**) ZNF274 PWM elicited from over 1500 highly reproducible BSs. (**B**) ENCODE ZNF-274 ChIP-Seq composite signal and peak calls at *SNORD116*-1, -3, -5, -7, -8, -9. Boxes below signal tracks indicate peak calls. The mapped positions of the elicited ZNF274 motif identified in A are indicated with a red line. The sequence shared by the 9 snoRNAs from Group I is indicated with a black line and the corresponding snoRNA is labeled with its number. (**C**) ZNF274 ChIP assays for cynomolgus stem cells.

Using the transiently expressed 116-Z-BS Guide 1 construct, we obtained two cell lines carrying ZNF274 BS mutations. BS-KO1 harbored a 20 bp deletion within BS5 encompassing 14 bp of the ZNF274 consensus binding motif (Figs 1 and 3A). BS-mod1 harbored a 9 bp deletion downstream of the BS6 binding motif (Fig. 1 and Supplementary Material, Fig. S1A). Using the constitutively expressed 116-Z-BS Guide 2, we obtained three cell lines carrying ZNF274 BS mutations. BS-KO2 carried a deletion encompassing BS1 to BS4, a 26 bp deletion at BS5 that included 17 bp of the ZNF274 consensus binding motif and a 7 bp insertion upstream of the ZNF274 consensus binding motif in BS6 that only affects the first 2 bp of the motif (Figs 1, 3A and Supplementary Material, Table S2). The second cell line, BS-mod2, harbored a deletion spanning BS4 to BS5 and a 6 bp insertion at BS6 that does not affect the ZNF274 consensus binding motif (Fig. 1 and Supplementary Material, Fig. S1A). The third cell line, BS-mod3, was found to have a 7 bp deletion at BS5 encompassing the first 5 bp of the ZNF274 consensus binding motif and a 14 bp insertion upstream of the ZNF274 consensus binding motif at BS6 that leaves the entire consensus binding motif intact (Fig. 1 and Supplementary Material, Fig. S1A).

Disruption of *ZNF274* binding sites depletes ZNF274 at the *SNORD116* locus

To determine whether mutating the ZNF274 consensus binding motif affected ZNF274 binding at *SNORD116*, we performed ChIP-qPCR for ZNF274 at BS5, BS6, and a non-*SNORD116* ZNF274 binding locus, *ZNF180* on the PWS iPSC lines carrying various mutations in the ZNF274 BSs. ChIP-qPCR for these sites were also performed on unedited PWS iPSCs, iPSCs derived from control individuals (CTRL1 and CTRL2) (37,45–47), and iPSCs from an AS patient carrying a large deletion of maternal chromosome 15q11–q13 (45) as controls. BS-KO1, BS-KO2 (Fig. 3B) and BS-mod2 (Supplementary Material, Fig. S1B) showed significantly decreased binding of ZNF274 at BS5, indicating that the BS5 consensus binding motif was severely disrupted or deleted in these cell lines. Conversely, BS-mod3, in

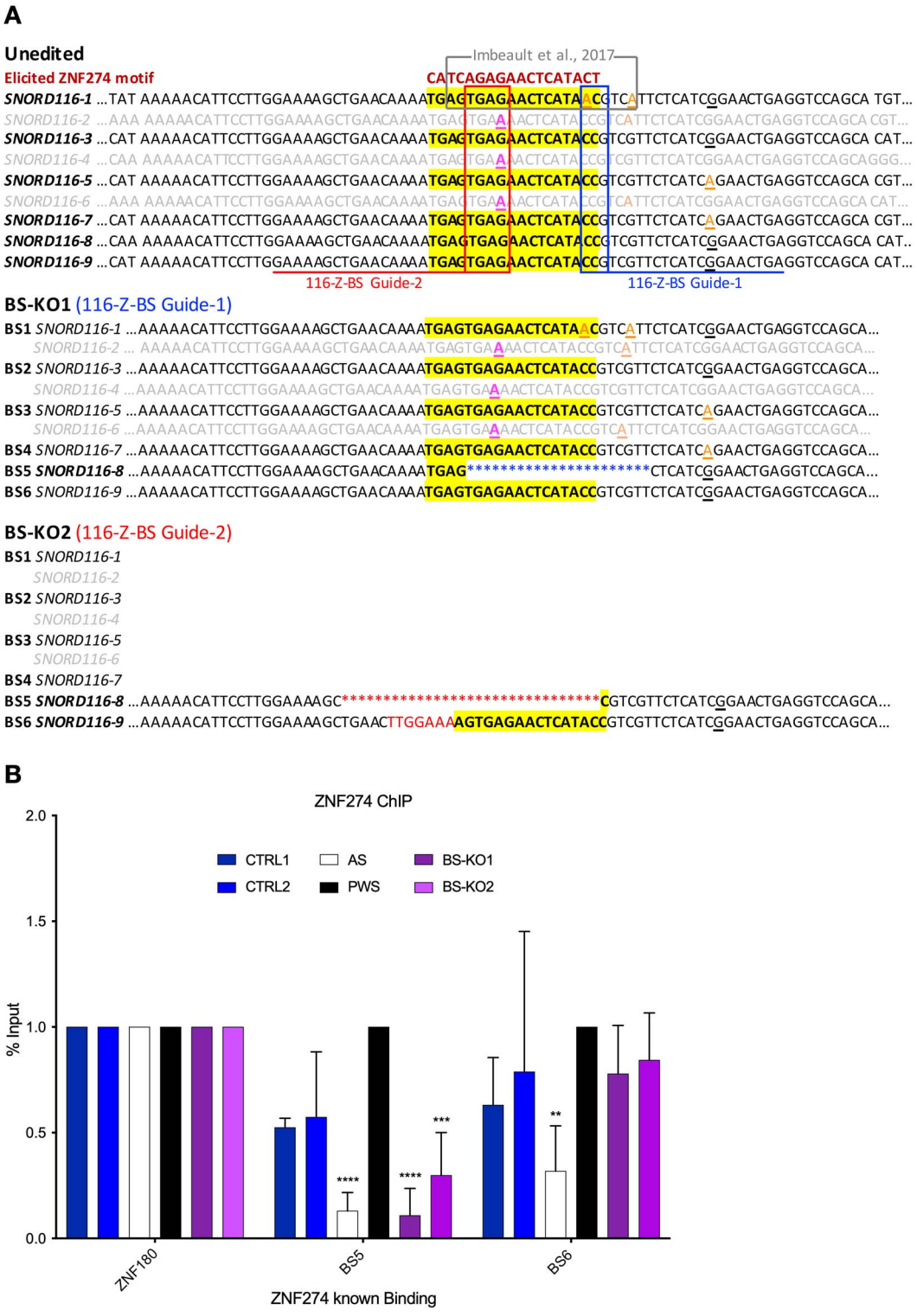

Figure 3. ZNF274 binding at *SNORD116*. (**A**) DNA sequences of portions of group 1 *SNORD116-1* through *SNORD116-9* are shown for the unedited condition in the first panel. The ZNF274 consensus sequence identified herein is highlighted in yellow. The position of the ZNF274 motif proposed by Imbeault *et al.* is indicated. *SNORD116* copies bound by ZNF274 are in black font, while those not bound by ZNF274 are in gray font. Single base substitutions are highlighted in colored fonts. The positions of gRNAs targeting ZNF274 BSs at *SNORD116* are underlined in blue and red. Their respective PAM sequences are in boxes. Lower panels illustrate the mutations incurred in the two BS-KO lines at each ZNF274 BS. (**B**) ChIP-qPCR for ZNF274 in iPSCs. Quantification of ChIP was performed and calculated as percent input for each sample. Binding at *ZNF180* is included as a positive control. Samples were normalized against the PWS (black) sample. A minimum of two biological replicates per cell line were performed: CTRL1 $n = 2$, CTRL2 $n = 3$, AS $n = 3$, PWS $n = 3$, BS-KO1 $n = 5$ and BS-KO2 $n = 3$. Significance was calculated using two-way ANOVA test with a Dunnett's post-test to compare the disrupted ZNF274 binding cell lines with PWS. $^{*}P < 0.05$, $^{**}P < 0.01$, $^{***}P < 0.001$, $^{****}P < 0.0001$.

which only the first 5 bp of the consensus sequence within BS5 was deleted, showed no significant difference in ZNF274 binding (Supplementary Material, Fig. S1B), indicating that deletion of the first 5 bp is not sufficient to disrupt ZNF274 binding. Using qPCR primers for BS6, there was no significant difference in ZNF274 binding for any of the cell lines, including BS-KO2, in which the first 2 bp of BS6 were deleted (Fig. 3B and Supplementary Material, Fig. S1B). For all mutant and control iPSCs, binding of the protein at the *ZNF180* 3′UTR was unaffected (Fig. 3B and Supplementary Material, Fig. S1B).

Disruption of *ZNF274* binding at *SNORD116* restores maternal gene expression in neurons

We first used RT-qPCR to determine whether disruption/deletion of ZNF274 BSs affected maternal gene expression in PWS iPSCs. We focused on cell lines carrying deletions of all or most of the ZNF274 consensus motifs. Similar to our previous observations in PWS iPSCs with ZNF274 knocked out (40), in BS-KO2, SNOG1del1 and SNOG2del2 iPSCs, we detected expression using probe-primer sets spanning exons U4 and exon 2 of *SNRPN*, but not exons 1 and 2, suggesting that the alternative upstream promoters but not the canonical promoter of *SNRPN* are activated (Fig. 4A). However, this activation of the upstream *SNRPN* exons did not lead to detectable *SNRPN* exon 3/4 or *116HGG2* expression in iPSCs, since the upstream *SNRPN* exons are known to be predominately expressed in neural cell types (40,47).

We next differentiated our engineered PWS iPSCs into neural progenitor cells (NPCs) and forebrain cortical neurons. Consistent with our previous observations quantifying maternal *SNHG14* RNAs in neurons differentiated from ZNF274 knockout iPSCs (LD KO1 and LD KO3), we saw more robust activation of *SNRPN* and *SNORD116* (*SNRPN* ex3/4 and *116HGG2*, respectively) upon neural differentiation of PWS iPSCs with disruptions/deletions in the ZNF274 BSs (Fig. 4B and C). In fact, expression levels of these transcripts in NPCs and neurons differentiated from ZNF274 BS mutated PWS iPSCs were approximately 50% of those seen in NPCs and neurons differentiated from neurotypical iPSCs. Furthermore, NPCs and neurons differentiated from the BS-KO2 PWS iPSCs, showed equivalent expression levels of these maternal *SNHG14* transcripts as neurons differentiated from SNOG1-del1 and −2 iPSCs. These data further support the hypothesis that ZNF274 binding at maternal *SNORD116* represses neuronal gene expression from the *SNRPN* and *SNHG14*. These data also suggest that ZNF274 binding to a single site within maternal *SNORD116* is not sufficient to maintain repression of this locus in PWS neurons.

In NPCs and neurons, expression of the *SNRPN* U4/exon 2 transcripts are fully restored by mutation of the ZNF274 BSs, while *SNRPN* transcripts that include exon 1 remain silent. Expression levels of the *SNRPN* U4/exon 2 transcripts in PWS NPCs and neurons with mutated ZNF274 BSs equal or exceed those seen in neurons differentiated from neurotypical iPSCs, while *SNRPN* exon 3/4 transcripts are only partially activated (Fig. 4B and C). These results are consistent with our previous work showing that the ZNF274 complex regulates neuronal *SNRPN/SNHG14* transcripts that are initiated from the *SNRPN* upstream promoters.

Disruption of ZNF274 binding also led to expression of *SNHG14* transcripts downstream of *SNORD116* (i.e. *UBE3A-ATS*; Fig. 4) in NPCs and neurons. *UBE3A-ATS* is known to silence paternal *UBE3A* in neurons. Neurons with disrupted ZNF274 BSs activate *UBE3A-ATS* to ∼50% of normal levels, and *UBE3A* expression is decreased to approximately 50% of normal levels (Fig. 4B and C). Complete *UBE3A-ATS*-mediated silencing of *UBE3A* may not be observed due to the relative immaturity of the neurons differentiated from the iPSCs. Alternatively, the increased expression of maternal *UBE3A* in PWS iPSC-derived neurons relative to their neurotypical counterparts may counteract the antisense-mediated silencing.

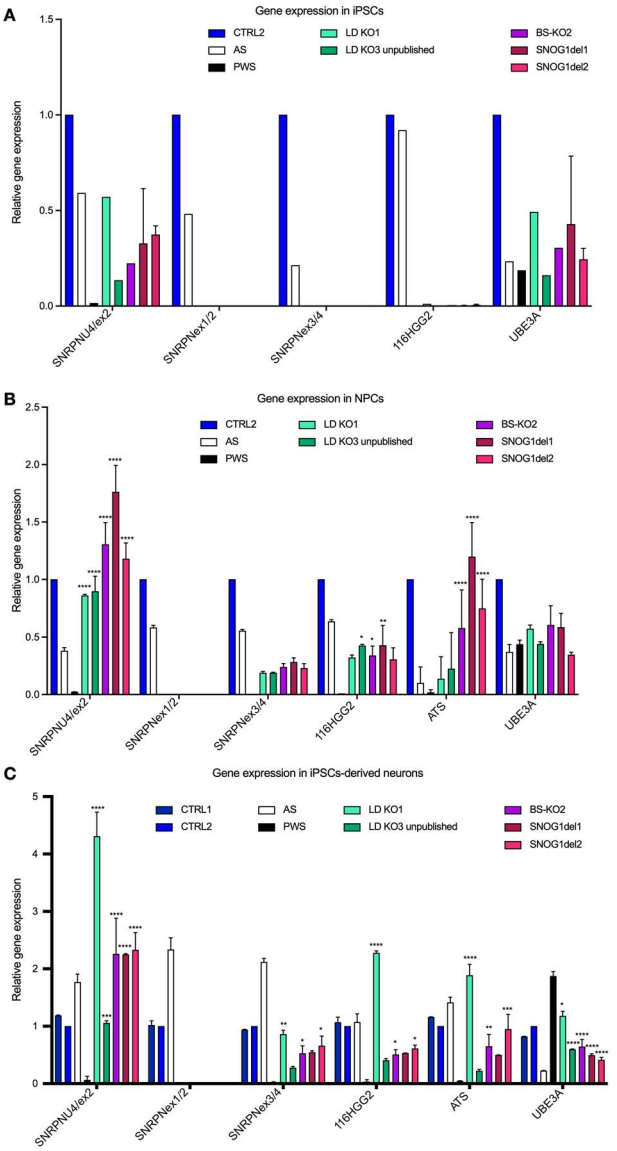

Figure 4. Disrupting ZNF274 binding at *SNORD116* activates transcription in PWS neurons. (**A**) Expression of the upstream *SNRPN* exons (U4/ex2), *SNRPN* major promoter (ex1/2), *SNRPN* mRNA (ex3/4), *SNORD116* Host Gene Group II (*116HGG2*) and *UBE3A* was quantified using RT-qPCR in (A). iPSCs ($n=1$ for all except SNOG1del1 and 2 with $n=5$ and $n=2$, respectively), (**B**) NPCs ($n=2$ for all except BS-KO2, SNOG1del1 and 2 with $n=3$, $n=3$ and $n=4$, respectively), and (**C**) neurons (CTRL1 $n=2$, CTRL2 $n=3$, AS $n=2$, PWS $n=2$, LD KO1 $n=2$, LD KO3 $n=2$, BS-KO2 $n=7$, SNOG1del1 $n=2$ and SNOG1del2 $n=3$). Expression of *UBE3A-ATS* was also quantified in NPCs and neurons in B and C, respectively. Gene expression was assessed using the comparative CT method with *GAPDH* as an endogenous control. Data were normalized to CTRL2 for each panel and plotted as the mean with SD. A minimum of two biological replicates per cell line were performed. Significance was calculated using two-way ANOVA test with a Dunnett's post-test to compare the disrupted ZNF274 binding cell lines with PWS. $^{*}P<0.05$, $^{**}P<0.01$, $^{***}P<0.001$, $^{****}P<0.0001$.

Discussion

PWS is caused by the loss of paternal gene expression from the chromosome 15q11–q13 locus. Since every individual with PWS has an intact copy of those genes on an epigenetically silenced maternal allele, activating those repressed genes is an attractive therapeutic strategy that addresses the root cause of PWS. The findings summarized here demonstrate that mutation of *ZNF274* consensus binding motifs within maternal *SNORD116* in PWS iPSCs leads to activation of *SNRPN* and *SNHG14* in neurons derived from them. This further supports the notion that prevention of ZNF274 binding at maternal *SNORD116* may be a viable therapeutic approach for PWS.

Identification of the ZNF274 consensus binding motif allowed us to map the precise nucleotides bound by ZNF274 and subsequently design CRISPR constructs to mutate them. Ideally, we would have been able to mutate individual ZNF274 BSs and identify the minimum number of disrupted sites required to activate *SNHG14* expression. However, our data suggest that BSs 5 and 6 are the most readily accessible by CRISPR/Cas9, and that deletions of multiple sites along with intervening DNA may be more likely to occur rather than mutating individual internal BSs (i.e. BS2–4). Sampling a larger number of mutated colonies generated by transiently expressing the 116-Z-BS Guide-1 construct would perhaps have yielded iPSCs harboring more individual BS mutations. Interestingly, the 116-Z-BS Guide 2 was less efficient at cutting and required constitutive expression via a lentiviral vector to generate mutated ZNF274 BSs. Although this approach yielded interesting iPSC lines, gene expression analyses from neurons differentiated from the more subtle BS mutations was not possible because these mutations were merely a snapshot in time, and each line would eventually accumulate more BS mutations until the gRNA binding was completely abolished from this locus. Similarly, some off-target effects are likely with this approach. Disruption of individual BSs may be possible with targeted dual CRISPR approaches to flank and delete individual sites one-by-one. Nonetheless, these data strongly suggest that BS5 and BS6 are the most accessible to CRISPR/Cas9.

PWS iPSCs with mutations of BS5 and BS6 allowed us to determine whether ZNF274 binding was disrupted by these mutations. Unsurprisingly, mutations that severely affected the BSs led to significantly reduced ZNF274 binding, but mutations that removed the first 2–5 bp of the BS did not significantly affect ZNF274 binding, although ChIP-seq in those iPSCs may provide more accurate quantification of ZNF274 binding in these lines. Interestingly, a G to A nucleotide change at position 8 of the ZNF274 consensus motif that occurs naturally within the human genome is sufficient to prevent ZNF274 binding. These data provide a start to understanding the critical nucleotides in the consensus binding sequence.

Most importantly, by mutating and/or deleting the ZNF274 consensus binding motifs, we demonstrated that it is feasible to deplete ZNF274 specifically within *SNORD116* (Fig. 3A and B). The loss of ZNF274 binding at this locus leads to the expression of maternal *SNHG14* in PWS iPSC-derived NPCs and neurons (Fig. 4). The expression levels of these activated transcripts approach normal levels and robust activation is observed not only within the *SNORD116* portion of *SNHG14*, but also extends throughout the proximal and distal portions of the *SNHG14* RNA, as shown by *SNRPN* and *UBE3A-ATS* expression (Fig. 4).

The canonical promoter of *SNRPN* was not activated by *ZNF274* binding disruption (Fig. 4). This was previously observed in PWS iPSCs carrying a full knockout of *ZNF274*, as well. We previously demonstrated that these ZNF274 knockout iPSCs did not have altered CpG methylation at the maternal PWS-IC compared with unedited PWS iPSCs. These data show that removal of ZNF274 binding at *SNORD116* does not affect DNA methylation at the PWS-IC and does not activate the canonical *SNRPN* promoter (40). Instead, disruption of ZNF274 binding at *SNORD116* leads to activation of upstream *SNRPN* promoters. These promoters are preferentially expressed in NPCs and neurons. We observe expression levels of upstream *SNRPN* transcripts in ZNF274 BS-mutated PWS NPCs and neurons that are similar to or even exceed those seen in neurotypical NPCs and neurons. These data further support the hypothesis that ZNF274 binding to maternal *SNORD116* serves as a somatic imprint to maintain repression of *SNRPN* and *SNHG14* in neural lineages.

As previously observed with our *ZNF274* knockout PWS neurons, we only detect a moderate decrease of *UBE3A* levels compared with control despite activation of *UBE3A-ATS* (Fig. 4). However, the level of expression of *UBE3A* in PWS neurons is substantially higher than normal control neurons. When compared with PWS neurons, *UBE3A* is reduced by more than 50% following *ZNF274* knockout (Fig. 4). We hypothesize that *UBE3A-ATS* is partially silencing maternal *UBE3A*, reducing it to levels just below those seen in control neurons. It is possible that full *UBE3A-ATS*-mediated silencing of *UBE3A* does not occur due to the relative immaturity of the neurons differentiated from the iPSCs compared with a fully developed brain. (45) However, it seems more likely that the relative expression levels of *UBE3A-ATS* and *UBE3A* in ZNF274 knockout neurons are balanced, resulting in the overall slight reduction in *UBE3A* compared with control neurons.

While it is clear that ZNF274 plays an important role in mediating the repression of the upstream *SNRPN* promoters in neurons, the specific histone methyltransferases and other co-factors involved are not as certain. We previously implicated the H3K9me3 histone methyltransferase, SETDB1, in this process and showed that PWS iPSCs with a knockdown of SETDB1 also activated maternal *SNHG14* and *SNRPN* (37). SETDB1 is a well-known partner of ZNF274 (38). Interestingly, Kim *et al.* successfully activated maternal *SNRPN* and *SNHG14* in human PWS fibroblasts and a mouse model of PWS, using novel compounds that inhibit the histone methyltransferase G9a (48,49). This activation of maternal PWS RNAs via G9a inhibition was linked to reduced levels of H3K9me3 and H3K9me2 at the *SNORD116* locus as well as reduced levels of H3K9me2 at the PWS-IC, without affecting DNA methylation levels at the PWS-IC (48). Similarly, Wu *et al.* showed activation of *SNHG14* and *SNRPN* in human PWS iPSC-derived NPCs and neurons using G9a inhibitors (https://www.biorxiv.org/content/10.1101/640938v1). Although the association of G9a with ZNF274 has not previously been shown, G9a and SETDB1 have been reported to complex together (50). Whether the G9a- and the ZNF274/SETDB1 complex-mediated H3K9me3 silencing of maternal chromosome 15q11–q13 transcripts are redundant or complimentary remains unknown. It will be important to determine the number of other genes affected by SETDB1, G9a and ZNF274 individually, and the extent to which the targets of these epigenetic regulators interact both to better understand the repressive mechanisms working on the *SNORD116* locus, but also to identify the potential pitfalls of SETDB1, G9a or ZNF274 inhibition as therapeutic approaches for PWS, such as affecting non-PWS related genes (41,51). Fortunately, our results show the feasibility of disrupting ZNF274 binding specifically at the maternal *SNORD116* locus. We hypothesize that this targeted approach will lead to restoration of appropriate *SNRPN/SNHG14*

gene expression without impacting other genes, providing a safer approach compared with inhibition of major epigenetic regulators. Further investigation into how to best prevent ZNF274 from binding at maternal *SNORD116* is needed to better define a potential strategy for future therapeutic application for PWS.

Material and Methods

Culture conditions of iPSCs and neuronal differentiation

iPSCs were grown on irradiated mouse embryonic fibroblasts and fed daily with conventional hESC medium composed of DMEM-F12 supplemented with knock-out serum replacer, non-essential amino acids, L-glutamine, β-mercaptoethanol and basic FGF. iPSCs were cultured in a humid incubator at 37°C with 5% CO_2 and manually passaged once a week (45).

Neuronal differentiation of iPSCs was performed using a monolayer differentiation protocol (52,53) with some modifications (45,46). Briefly, iPSC colonies were cultured in hESC medium for 24 h before switching to N2B27 medium. Cells were fed every other day with N2B27 medium containing Neurobasal Medium, 2% B-27 supplement, 2 mM L-glutamine, 1% Insulin-transferrin-selenium, 1% N2 supplement, 0.5% Pen-strep and was supplemented with fresh noggin at 500 ng/ml. After three weeks of neural differentiation, neural progenitors were plated on tissue culture plates coated with poly-ornithine/laminin. The neural differentiation medium consisted of Neurobasal Medium, B-27 supplement, non-essential amino acids and L-glutamine, and was supplemented with 1 µM ascorbic acid, 200 µM cyclic adenosine monophosphate, 10 ng/ml brain-derived neurotrophic factor and 10 ng/ml glial-derived neurotrophic factor. Unless otherwise specified, cells were harvested once neural cultures reached at least 10 weeks of age.

Lentiviral production, transduction and clone screening

sgRNAs were designed using a web-based CRISPR design tool and cloned into lentiCRISPR (Addgene Plasmid 49 535 and 52 961) original or modified to create the VQR mutation, lentiGuidePuro (Addgene Plasmid 52 963) or pX459 v2.0 (Addgene plasmid 62 988) using our standard protocol (54–56). Lentiviral particles were made by transfecting 293FT cells with second generation packaging systems using Lipofectamine 2000 (Life Technologies). Prior to transduction or electroporation, iPSCs were treated with 10 µM ROCK inhibitor, Y-27632, overnight. The next day, iPSCs were singlized using Accutase (Millipore) before transduction/electroporation. Transduction was done with lentivirus in suspension in the presence of 8 µg/ml polybrene in a low-attachment dish for 2 h. Then, the iPSCs/lentivirus mixture was diluted 1:1 in hESC medium before plating. Electroporation was performed in 0.4 cm cuvettes loaded with 10 µg of the CRISPR/Cas9 and 800 µl of PBS suspended iPSCs. Cells were electroporated with plasmids expressing gRNAs as well as Cas9 and a puromycin resistance cassette, using a Biorad Gene Pulser X Cell with the exponential protocol, at 250 V, a 500 µF capacitance, ∞ resistance. Transduced/electroporated cells were plated on puromycin-resistant (DR4) MEF feeders at a low density, supplemented with 10 µM ROCK inhibitor, Y-27632, overnight. Following transient delivery of SNOG1del Guide-1, SNOG1del Guide-2 and 116-Z-BS Guide 1 and lentiviral delivery of 116-Z-BS Guide 2, puromycin selection was used to eliminate iPSCs that had not received the CRISPR construct. Following transduction, attached cells were cultured in hESC medium for an additional 72 h before starting drug selection using puromycin at 0.5 µg/ml during the first week and at 1 µg/ml during the second week. Following electroporation, at 24 h post plating, the cells were transiently selected with 0.5 µg/ml of puromycin for a total of 48 h. Puromycin-resistant iPSC colonies were individually picked into a new feeder well and screened for indels by performing conventional PCR on genomic DNA and Sanger sequencing for each of the six BSs. Primers flanking the intended CRISPR cut sites were used to identify cells harboring a deletion, whereas primers located between the intended cut sites were used to determine whether colonies with the deletion were mixed (i.e. contained both deletion and non-deletion cells).

The sgRNA sequences and PAM are summarized in Supplementary Material, Table S1. The genetic alterations induced are detailed in Figures 1, 3A and Supplementary Material, Figure S1A. The cell lines are summarized in Supplementary Material, Table S2. PCR primers used to amplify the desired genomic regions are summarized in Supplementary Material, Table S3.

RNA isolation and RT reaction

RNA was isolated from cells using RNA-Bee (Tel Test, Inc.). Samples were DNase-treated as needed with Amplification Grade DNaseI (Invitrogen) at 37°C for 45 min, and cDNA was synthesized using the High Capacity cDNA Reverse Transcription Kit (Life Technologies) according to the manufacturer's instructions.

RT-qPCR and expression arrays

For single gene expression assays, expression levels of target genes were examined using TaqMan Gene Expression Assays (Applied Biosystems) on the Step One Plus (ThermoFisher Scientific) or on the BioRAD CFX96 Real Time PCR system (Biorad). An amount of RT reaction corresponding to 30 ng of RNA was used in a volume of 20ul per reaction. Reactions were performed in technical duplicates or triplicates and the *GAPDH* Endogenous Control TaqMan Assay was used as an endogenous control, following the manufacturer's protocol. Relative quantity (RQ) value was calculated as $2^{-\Delta\Delta Ct}$ using the normal cell lines CTRL1 or CTRL2 as the calibrator sample.

Chromatin immunoprecipitation

Chromatin immunoprecipitation (ChIP) assays were performed as described before (37,40,57,58). The antibody anti-ZNF274 (Abnova, Cat# H00010782-M01) was used. Quantification of ChIPs was performed using SYBR Green quantitative PCR. PCR primers used to amplify the purified DNA can be found in Supplementary Material, Table S3. The enrichment of the DNA was calculated as percent input, as described. (58) Normal rabbit IgG was used for the isotype controls and showed no enrichment. Data were presented as means with SD and represent the average of at least two biological replicates from independent cultures.

Statistical tests

Statistical analysis was carried out using Prism software (GraphPad). For each condition shown, averaged values from a minimum of two biological replicates from independent cultures were calculated and the resulting standard deviation (SD) was reported in the error bars. Unless otherwise specified, for each experiment, averaged values for each sample were compared

with that of the parental PWS cell line of the same genotype (PWS LD) and the significance for each un-manipulated versus KO pair was calculated using the one- or two-way analysis of variance (ANOVA) with the Dunnett's post-test.

Supplementary Material

Supplementary Material is available at *HMG* online.

Web Resources

UCSC Human Genome Browser, http://genome.ucsc.edu/cgi-bin/hgGateway

Web-based CRISPR design tool, http://crispr.mit.edu

TIDE: method for easy quantitative assessment of genome editing, https://tide.nki.nl/

CRISP-ID: Detecting CRISPR mediated indels by Sanger sequencing, http://crispid.gbiomed.kuleuven.be/

RoadMap Epigenomics, http://egg2.wustl.edu/roadmap/web_portal/imputed.html#imp_sig

Acknowledgements

We thank David S. Rosenblatt, Gail Dunbar and Daniel J. Driscoll for patient clinical evaluation and information, and for providing skin biopsies/fibroblasts. We thank James A. Thomson, John P. Maufort, Elizabeth S. Perrin and Jessica Antosiewicz-Bourget at Wisconsin National Primate Research Center, University of Wisconsin–Madison for the cynomolgus iPSCs and for technical assistance with cynomolgus iPSCs culture.

Conflict of Interest statement. The authors declare no competing financial interests.

Funding

Foundation for Prader-Willi Research (to M. Lalande), Connecticut Regenerative Medicine Research Fund (to M. Lalande), Cascade Fellowship (to M. Langouet), Levo Therapeutics (to SC), and National Institutes of Health grant HD099975 (to SC and JC).

Author Contributions

M.L. and J.C. analyzed the ChIP-seq data and J.C. identified the consensus binding motif for ZNF274. M.L., C.O., C.D.T., H.G.D. and C.S. designed and tested the CRISPR/gRNAs. M.L., C.O. and D.G. screened and generated the engineered cell lines. M.L., C.O., D.G., M.C. and L.C. characterized the engineered cell lines. M.L. executed and analyzed ChIP data from human iPSCs. M.C. executed and analyzed ChIP data from Cynomolgus stem cells. M.L., N.G. and D.G. performed neuronal differentiation. M.L. and D.G. performed and analyzed the gene expression assays. M.L. executed statistical analysis of the data. M.L., C.S., S.C. and M. Lalande designed and directed the study. All authors contributed to writing and editing the manuscript.

References

1. Angulo, M.A., Butler, M.G. and Cataletto, M.E. (2015) Prader-Willi syndrome: a review of clinical, genetic, and endocrine findings. *J. Endocrinol. Investig.*, **38**, 1249–1263.
2. Cassidy, S.B., Schwartz, S., Miller, J.L. and Driscoll, D.J. (2012) Prader-Willi syndrome. *Genet. Med.*, **14**, 10–26.
3. Edge, R., la Fleur, P. and Adcock, L. (2018) *Human Growth Hormone Treatment for Children with Prader-Willi Syndrome: A Review of Clinical Effectiveness, Cost-Effectiveness, and Guidelines*, Ottawa (ON): Canadian Agency for Drugs and Technologies in Health; 2018 Jan 25.
4. Moix Gil, E., Gimenez-Palop, O. and Caixas, A. (2018) Treatment with growth hormone in the prader-willi syndrome. *Endocrinol. Diabetes Nutr.*, **65**, 229–236.
5. Pullen, L.C., Picone, M., Tan, L., Johnston, C. and Stark, H. (2019) Cognitive improvements in children with Prader-Willi syndrome following Pitolisant treatment-patient reports. *J. Pediatr. Pharmacol. Ther.*, **24**, 166–171.
6. Carias, K.V. and Wevrick, R. (2019) Preclinical testing in translational animal models of Prader-Willi syndrome: overview and gap analysis. *Mol. Ther. Methods Clin. Dev.*, **13**, 344–358.
7. Kabasakalian, A., Ferretti, C.J. and Hollander, E. (2018) Oxytocin and Prader-Willi syndrome. *Curr. Top. Behav. Neurosci.*, **35**, 529–557.
8. Rice, L.J., Einfeld, S.L., Hu, N. and Carter, C.S. (2018) A review of clinical trials of oxytocin in Prader-Willi syndrome. *Curr. Opin. Psychiatry*, **31**, 123–127.
9. Cavaille, J., Buiting, K., Kiefmann, M., Lalande, M., Brannan, C.I., Horsthemke, B., Bachellerie, J.P., Brosius, J. and Huttenhofer, A. (2000) Identification of brain-specific and imprinted small nucleolar RNA genes exhibiting an unusual genomic organization. *Proc. Natl. Acad. Sci. USA*, **97**, 14311–14316.
10. Dittrich, B., Buiting, K., Korn, B., Rickard, S., Buxton, J., Saitoh, S., Nicholls, R.D., Poustka, A., Winterpacht, A., Zabel, B. *et al.* (1996) Imprint switching on human chromosome 15 may involve alternative transcripts of the SNRPN gene. *Nat. Genet.*, **14**, 163–170.
11. Farber, C., Dittrich, B., Buiting, K. and Horsthemke, B. (1999) The chromosome 15 imprinting Centre (IC) region has undergone multiple duplication events and contains an upstream exon of SNRPN that is deleted in all Angelman syndrome patients with an IC microdeletion. *Hum. Mol. Genet.*, **8**, 337–343.
12. Landers, M., Bancescu, D.L., Le Meur, E., Rougeulle, C., Glatt-Deeley, H., Brannan, C., Muscatelli, F. and Lalande, M. (2004) Regulation of the large (approximately 1000 kb) imprinted murine Ube3a antisense transcript by alternative exons upstream of Snurf/Snrpn. *Nucleic Acids Res.*, **32**, 3480–3492.
13. Lewis, M.W., Brant, J.O., Kramer, J.M., Moss, J.I., Yang, T.P., Hansen, P.J., Williams, R.S. and Resnick, J.L. (2015) Angelman syndrome imprinting center encodes a transcriptional promoter. *Proc. Natl. Acad. Sci. USA*, **112**, 6871–6875.
14. Meng, L., Person, R.E. and Beaudet, A.L. (2012) Ube3a-ATS is an atypical RNA polymerase II transcript that represses the paternal expression of Ube3a. *Hum. Mol. Genet.*, **21**, 3001–3012.
15. Numata, K., Kohama, C., Abe, K. and Kiyosawa, H. (2011) Highly parallel SNP genotyping reveals high-resolution landscape of mono-allelic Ube3a expression associated with locus-wide antisense transcription. *Nucleic Acids Res.*, **39**, 2649–2657.
16. Rougeulle, C., Cardoso, C., Fontes, M., Colleaux, L. and Lalande, M. (1998) An imprinted antisense RNA overlaps UBE3A and a second maternally expressed transcript. *Nat. Genet.*, **19**, 15–16.
17. Runte, M., Huttenhofer, A., Gross, S., Kiefmann, M., Horsthemke, B. and Buiting, K. (2001) The IC-SNURF-SNRPN transcript serves as a host for multiple small nucleolar RNA species and as an antisense RNA for UBE3A. *Hum. Mol. Genet.*, **10**, 2687–2700.

18. Castle, J.C., Armour, C.D., Lower, M., Haynor, D., Biery, M., Bouzek, H., Chen, R., Jackson, S., Johnson, J.M., Rohl, C.A. *et al*. (2010) Digital genome-wide ncRNA expression, including SnoRNAs, across 11 human tissues using polyA-neutral amplification. *PLoS One*, **5**, e11779.
19. Buiting, K., Saitoh, S., Gross, S., Dittrich, B., Schwartz, S., Nicholls, R.D. and Horsthemke, B. (1995) Inherited microdeletions in the Angelman and Prader-Willi syndromes define an imprinting Centre on human chromosome 15. *Nat. Genet*., **9**, 395–400.
20. Cavaille, J. (2017) Box C/D small nucleolar RNA genes and the Prader-Willi syndrome: a complex interplay. *Wiley Interdiscip. Rev. RNA*, **8**, e1417.
21. Garfield, A.S., Davies, J.R., Burke, L.K., Furby, H.V., Wilkinson, L.S., Heisler, L.K. and Isles, A.R. (2016) Increased alternate splicing of Htr2c in a mouse model for Prader-Willi syndrome leads disruption of 5HT2C receptor mediated appetite. *Mol. Brain*, **9**, 95.
22. Kishore, S. and Stamm, S. (2006) The snoRNA HBII-52 regulates alternative splicing of the serotonin receptor 2C. *Science*, **311**, 230–232.
23. Bratkovic, T., Modic, M., Camargo Ortega, G., Drukker, M. and Rogelj, B. (2018) Neuronal differentiation induces SNORD115 expression and is accompanied by post-transcriptional changes of serotonin receptor 2c mRNA. *Sci. Rep*., **8**, 5101.
24. Doe, C.M., Relkovic, D., Garfield, A.S., Dalley, J.W., Theobald, D.E., Humby, T., Wilkinson, L.S. and Isles, A.R. (2009) Loss of the imprinted snoRNA mbii-52 leads to increased 5htr2c pre-RNA editing and altered 5HT2CR-mediated behaviour. *Hum. Mol. Genet*., **18**, 2140–2148.
25. Raabe, C.A., Voss, R., Kummerfeld, D.M., Brosius, J., Galiveti, C.R., Wolters, A., Seggewiss, J., Huge, A., Skryabin, B.V. and Rozhdestvensky, T.S. (2019) Ectopic expression of Snord115 in choroid plexus interferes with editing but not splicing of 5-Ht2c receptor pre-mRNA in mice. *Sci. Rep*., **9**, 4300.
26. Keshavarz, M., Krebs-Wheaton, R., Refki, P., Savriama, Y., Zhang, Y., Guenther, A., Brückl, T.M., Binder, E.B. and Tautz, D. (2020) Copy number variation in small nucleolar RNAs regulates personality behavior. *bioRxiv*. doi: 10.1101/476010.
27. Bieth, E., Eddiry, S., Gaston, V., Lorenzini, F., Buffet, A., Conte Auriol, F., Molinas, C., Cailley, D., Rooryck, C., Arveiler, B. *et al*. (2015) Highly restricted deletion of the SNORD116 region is implicated in Prader-Willi syndrome. *Eur. J. Hum. Genet*., **23**, 252–255.
28. de Smith, A.J., Purmann, C., Walters, R.G., Ellis, R.J., Holder, S.E., Van Haelst, M.M., Brady, A.F., Fairbrother, U.L., Dattani, M., Keogh, J.M. *et al*. (2009) A deletion of the HBII-85 class of small nucleolar RNAs (snoRNAs) is associated with hyperphagia, obesity and hypogonadism. *Hum. Mol. Genet*., **18**, 3257–3265.
29. Duker, A.L., Ballif, B.C., Bawle, E.V., Person, R.E., Mahadevan, S., Alliman, S., Thompson, R., Traylor, R., Bejjani, B.A., Shaffer, L.G. *et al*. (2010) Paternally inherited microdeletion at 15q11.2 confirms a significant role for the SNORD116 C/D box snoRNA cluster in Prader-Willi syndrome. *Eur. J. Hum. Genet*., **18**, 1196–1201.
30. Sahoo, T., del Gaudio, D., German, J.R., Shinawi, M., Peters, S.U., Person, R.E., Garnica, A., Cheung, S.W. and Beaudet, A.L. (2008) Prader-Willi phenotype caused by paternal deficiency for the HBII-85 C/D box small nucleolar RNA cluster. *Nat. Genet*., **40**, 719–721.
31. Ding, F., Li, H.H., Zhang, S., Solomon, N.M., Camper, S.A., Cohen, P. and Francke, U. (2008) SnoRNA Snord116 (Pwcr1/MBII-85) deletion causes growth deficiency and hyperphagia in mice. *PLoS One*, **3**, e1709.
32. Qi, Y., Purtell, L., Fu, M., Lee, N.J., Aepler, J., Zhang, L., Loh, K., Enriquez, R.F., Baldock, P.A., Zolotukhin, S. *et al*. (2016) Snord116 is critical in the regulation of food intake and body weight. *Sci. Rep*., **6**, 18614.
33. Skryabin, B.V., Gubar, L.V., Seeger, B., Pfeiffer, J., Handel, S., Robeck, T., Karpova, E., Rozhdestvensky, T.S. and Brosius, J. (2007) Deletion of the MBII-85 snoRNA gene cluster in mice results in postnatal growth retardation. *PLoS Genet*., **3**, e235.
34. Polex-Wolf, J., Lam, B.Y., Larder, R., Tadross, J., Rimmington, D., Bosch, F., Cenzano, V.J., Ayuso, E., Ma, M.K., Rainbow, K. *et al*. (2018) Hypothalamic loss of Snord116 recapitulates the hyperphagia of Prader-Willi syndrome. *J. Clin. Invest*., **128**, 960–969.
35. Burnett, L.C., LeDuc, C.A., Sulsona, C.R., Paull, D., Rausch, R., Eddiry, S., Carli, J.F., Morabito, M.V., Skowronski, A.A., Hubner, G. *et al*. (2017) Deficiency in prohormone convertase PC1 impairs prohormone processing in Prader-Willi syndrome. *J. Clin. Invest*., **127**, 293–305.
36. Polex-Wolf, J., Yeo, G.S. and O'Rahilly, S. (2017) Impaired prohormone processing: a grand unified theory for features of Prader-Willi syndrome? *J. Clin. Invest*., **127**, 98–99.
37. Cruvinel, E., Budinetz, T., Germain, N., Chamberlain, S., Lalande, M. and Martins-Taylor, K. (2014) Reactivation of maternal SNORD116 cluster via SETDB1 knockdown in Prader-Willi syndrome iPSCs. *Hum. Mol. Genet*., **23**, 4674–4685.
38. Frietze, S., O'Geen, H., Blahnik, K.R., Jin, V.X. and Farnham, P.J. (2010) ZNF274 recruits the histone methyltransferase SETDB1 to the 3′ ends of ZNF genes. *PLoS One*, **5**, e15082.
39. Witzgall, R., O'Leary, E., Leaf, A., Onaldi, D. and Bonventre, J.V. (1994) The Kruppel-associated box-A (KRAB-A) domain of zinc finger proteins mediates transcriptional repression. *Proc. Natl. Acad. Sci. USA*, **91**, 4514–4518.
40. Langouet, M., Glatt-Deeley, H.R., Chung, M.S., Dupont-Thibert, C.M., Mathieux, E., Banda, E.C., Stoddard, C.E., Crandall, L. and Lalande, M. (2018) Zinc finger protein 274 regulates imprinted expression of transcripts in Prader-Willi syndrome neurons. *Hum. Mol. Genet*., **27**, 505–515.
41. Valle-Garcia, D., Qadeer, Z.A., McHugh, D.S., Ghiraldini, F.G., Chowdhury, A.H., Hasson, D., Dyer, M.A., Recillas-Targa, F. and Bernstein, E. (2016) ATRX binds to atypical chromatin domains at the 3′ exons of zinc finger genes to preserve H3K9me3 enrichment. *Epigenetics*, **11**, 398–414.
42. Bailey, T.L., Williams, N., Misleh, C. and Li, W.W. (2006) MEME: discovering and analyzing DNA and protein sequence motifs. *Nucleic Acids Res*., **34**, W369–W373.
43. Grant, C.E., Bailey, T.L. and Noble, W.S. (2011) FIMO: scanning for occurrences of a given motif. *Bioinformatics*, **27**, 1017–1018.
44. Imbeault, M., Helleboid, P.Y. and Trono, D. (2017) KRAB zinc-finger proteins contribute to the evolution of gene regulatory networks. *Nature*, **543**, 550–554.
45. Chamberlain, S.J., Chen, P.F., Ng, K.Y., Bourgois-Rocha, F., Lemtiri-Chlieh, F., Levine, E.S. and Lalande, M. (2010) Induced pluripotent stem cell models of the genomic imprinting disorders Angelman and Prader-Willi syndromes. *Proc. Natl. Acad. Sci. USA*, **107**, 17668–17673.
46. Germain, N.D., Chen, P.F., Plocik, A.M., Glatt-Deeley, H., Brown, J., Fink, J.J., Bolduc, K.A., Robinson, T.M., Levine, E.S., Reiter, L.T. *et al*. (2014) Gene expression analysis of human induced pluripotent stem cell-derived neurons carrying copy number variants of chromosome 15q11-q13.1. *Mol. Autism*, **5**, 44.

47. Martins-Taylor, K., Hsiao, J.S., Chen, P.F., Glatt-Deeley, H., De Smith, A.J., Blakemore, A.I., Lalande, M. and Chamberlain, S.J. (2014) Imprinted expression of UBE3A in non-neuronal cells from a Prader-Willi syndrome patient with an atypical deletion. *Hum. Mol. Genet.*, **23**, 2364–2373.
48. Kim, Y., Lee, H.M., Xiong, Y., Sciaky, N., Hulbert, S.W., Cao, X., Everitt, J.I., Jin, J., Roth, B.L. and Jiang, Y.H. (2017) Targeting the histone methyltransferase G9a activates imprinted genes and improves survival of a mouse model of Prader-Willi syndrome. *Nat. Med.*, **23**, 213–222.
49. Kim, Y., Wang, S.E. and Jiang, Y.H. (2019) Epigenetic therapy of Prader-Willi syndrome. *Transl. Res.*, **208**, 105–118.
50. Fritsch, L., Robin, P., Mathieu, J.R., Souidi, M., Hinaux, H., Rougeulle, C., Harel-Bellan, A., Ameyar-Zazoua, M. and Ait-Si-Ali, S. (2010) A subset of the histone H3 lysine 9 methyltransferases Suv39h1, G9a, GLP, and SETDB1 participate in a multimeric complex. *Mol. Cell*, **37**, 46–56.
51. Avgustinova, A., Symeonidi, A., Castellanos, A., Urdiroz-Urricelqui, U., Sole-Boldo, L., Martin, M., Perez-Rodriguez, I., Prats, N., Lehner, B., Supek, F. *et al.* (2018) Loss of G9a preserves mutation patterns but increases chromatin accessibility, genomic instability and aggressiveness in skin tumours. *Nat. Cell Biol.*, **20**, 1400–1409.
52. Banda, E. and Grabel, L. (2016) Directed differentiation of human embryonic stem cells into neural progenitors. *Methods Mol. Biol.*, **1307**, 289–298.
53. Germain, N.D., Banda, E.C., Becker, S., Naegele, J.R. and Grabel, L.B. (2013) Derivation and isolation of NKX2.1-positive basal forebrain progenitors from human embryonic stem cells. *Stem Cells Dev.*, **22**, 1477–1489.
54. Chen, P.F., Hsiao, J.S., Sirois, C.L. and Chamberlain, S.J. (2016) RBFOX1 and RBFOX2 are dispensable in iPSCs and iPSC-derived neurons and do not contribute to neural-specific paternal UBE3A silencing. *Sci. Rep.*, **6**, 25368.
55. Sanjana, N.E., Shalem, O. and Zhang, F. (2014) Improved vectors and genome-wide libraries for CRISPR screening. *Nat. Methods*, **11**, 783–784.
56. Shalem, O., Sanjana, N.E., Hartenian, E., Shi, X., Scott, D.A., Mikkelsen, T.S., Heckl, D., Ebert, B.L., Root, D.E., Doench, J.G. *et al.* (2014) Genome-scale CRISPR-Cas9 knockout screening in human cells. *Science*, **343**, 84–87.
57. Cotney, J.L. and Noonan, J.P. (2015) Chromatin immunoprecipitation with fixed animal tissues and preparation for high-throughput sequencing. *Cold Spring Harb. Protoc.*, **2015**, 191–199.
58. Martins-Taylor, K., Schroeder, D.I., LaSalle, J.M., Lalande, M. and Xu, R.H. (2012) Role of DNMT3B in the regulation of early neural and neural crest specifiers. *Epigenetics*, **7**, 71–82.